Suppression of the Polarization Dependence of the Vertical Photoluminescence from InAs/GaAs Quantum Dots by InGaAs Strain-reducing Layer

Kohki Mukai* and Kenta Nakashima

Division of Materials Science and Engineering, Yokohama National University,

79-5 Tokiwadai, Hodogaya-Ku, Yokohama 240-8501, Japan

*Email address : mukai@ynu.ac.jp

Abstract

We report the linear polarization features of the vertical photoluminescence from InAs/GaAs self-assembled quantum dots (QDs) embedded in an InGaAs strain-reducing layer. The QD samples were grown by molecular beam epitaxy. We observed the polarization dependence of the vertical photoluminescence intensity that is expected to originate in the in-plane asymmetry of the QD structure. The polarization dependence of the photoluminescence intensity of the QDs was suppressed by increasing the indium composition and the thickness of the strain-reducing layer. We computed the electron wavefunction based on the three-dimensional finite element method to explain the results of the experiments. We found that the symmetry of the wavefunction in the embedded QD is superior to that of the crystallographic QD structure, and that the improvement is attributed to the

asymmetric permeation of the wavefunction into the strain-reducing layer. These results will aid in the development of vertical-light-emitting QD devices such as surface-emitting lasers and entangled-photon generators.

KEYWORDS : quantum dot, polarization, strain-reducing layer, symmetry, wavefunction

1. Introduction

It is of great interest to control the shape of self-assembled quantum dots (QDs) for use in optical telecommunication and quantum information processing. In optoelectronic QD devices, the symmetry of the QD shape affects the optical polarization characteristics. To control the polarization dependence of stripe lasers and semiconductor optical amplifiers, columnar-shaped QDs, which are grown by stacking small QDs in the growth direction, have been reported to be advantageous.[1,2] The symmetric shape of these QDs in the lateral direction is a key to their advantage. The polarization of photoemission depends on the carrier confinement direction within the QD structure.[3] We have reported a computational study in which the Stranski-Krastanow (SK)-type flat QD structure exhibited improved lateral electron wavefunction symmetry when embedded in a strain-reducing layer.[4] This improvement arises because the crystal lattice of the QD is expanded in the vertical direction into the strain-reducing layer,[5] which results in a reduction of the strength of quantum confinement and the consequent vertical expansion of the wavefunction into the strain-reducing layer.

The in-plane symmetry of QDs is also important for the application of optoelectronic QD devices that use vertical light emission. The polarization features of surface-emitting QD lasers will depend on the QD's in-plane symmetry. The in-plane symmetry is also important for the devices applied in quantum communication and

quantum computation. Semiconductor QD devices for the generation of single photons and entangled-photon pairs have been eagerly studied, and the reported quantum-information devices are designed to launch photons vertically into the free air space using vertical micro-cavities with QDs.[6, 7] The SK-type flat QD is not symmetric in the horizontal direction and is elongated in the [1 -1 0] direction on a (001) substrate.[8-11] Symmetry of the wavefunction in the QD state is critical for generating entangled-photon pairs using biexciton emission because a pair of generation processes for two polarized photons need to be undistinguishable.[12, 13] Due to the asymmetric QD shape, a QD has not produced entangled-photon pairs.[14]

In this paper, we report the linear polarization features of the vertical photoluminescence from InAs/GaAs self-assembled QDs embedded in an InGaAs strain-reducing layer. This QD structure has been widely studied for developing long-wavelength telecommunication applications.[15, 16] We studied the dependence of the polarization of photoluminescence intensity on the indium composition and thickness of the strain-reducing layer. The experimental results were compared with the computed results for the in-plane aspect ratio of electron wavefunction in the QDs. The permeation of the wavefunction into the vicinity of the QD is discussed in relation to the structural parameters of the strain-reducing layer to explain the improvement of in-plane symmetry.

2. Experiments and Results

The SK-type QD samples were prepared using molecular beam epitaxy (MBE). The samples were grown on (001)-GaAs substrates at 510°C. The dots were covered by an $In_xGa_{1-x}As$ strain-reducing layer and then capped by a 100-nm GaAs layer. The thickness of the strain-reducing layer was 0 - 12 nm. The indium composition of the strain-reducing layer, x, was also varied from 0 to 0.19. Figure 1(a) shows a bright-field cross-sectional transmission electron microscope (TEM) image of one QD embedded in a 12-nm $In_{0.17}Ga_{0.83}As$ strain-reducing layer. We can see that the diameter of the dark QD area is about 30 nm, and that the height is almost the same as that of the strain-reducing layer. Figure 1(b) shows a dark-field cross-sectional TEM image of the same area shown in Fig. 1(a). The dark-field image is sensitive to the distribution of component elements. We found that the actual QD size is smaller than that shown in Fig. 1(a). The QD seems to be domed, and the crystal distortion spreads into the strain-reducing layer. Based on the TEM observation of the samples, we concluded that the QD was 25-30 nm in diameter and 8-10 nm in height.

The photoluminescence perpendicular to the sample surface was observed at room temperature with a 633-nm He-Ne laser as the pump. The polarization dependence of the luminescence was investigated by placing a linear polarizer in front of a 20-cm monochromator. An InGaAs photomultiplier detector cooled to -80°C was used as the detector. We compared the photoluminescence spectra in the most intense

polarization direction with that in the 90°-rotated direction. To eliminate the polarization dependence of the measurement system, a depolarizer was integrated into the system behind the polarizer.

Figures 2(a) and 2(b) show the photoluminescence spectra of samples with various indium compositions and strain-reducing layer thicknesses, respectively. The main peak is the ground level, and the peaks immediately to the left of the main peak are expected to be the first excited level. The spectra for the two polarization directions were compared. The most intense polarization direction is expected to agree with the direction of the major axis of the asymmetric QD structure. Figure 2(a) shows the results when the sample thickness was 8 nm. We see that the higher the indium composition of the strain-reducing layer, the longer the emission peak wavelength, and the lower the emission intensity. We could not observe the luminescence of the samples when the indium composition of the strain-reducing layer, x, was 0.19. The emission wavelengths for the two polarization directions were almost the same, but they obviously changed at x = 0.15 and 0.17. Figure 2(b) shows the results when the thickness of the strain-reducing layer, d, varied at x = 0.17. The thicker the strain-reducing layer, the weaker the emission intensity. We could not observe the luminescence of the samples with a 12-nm-thick strain-reducing layer. The thickness of the strain-reducing layer had a complicated influence on the emission wavelength. The peak emission wavelength was the longest at d = 6 nm, but was almost the same

for the InGaAs-embedded samples. At d = 8 and 10 nm, the emission peaks changed with the polarization direction. The behavior of the emission wavelength may be due to the structure of the sublevels in the asymmetric QD, but the mechanism is not well understood at present.

We found that the strain-reducing layer effectively suppressed the polarization dependence of the photoluminescence intensity. Figure 3(a) shows the photoluminescence intensities in the two polarization directions, $I_{PL}^{0^\circ}$ and $I_{PL}^{90^\circ}$, and their ratio, $I_{PL}^{90^\circ}/I_{PL}^{0^\circ}$, as a function of the indium composition of the strain-reducing layer. We found that $I_{PL}^{90^\circ}/I_{PL}^{0^\circ}$ increased as the indium composition of the strain-reducing layer was raised to 0.17. The increase was not linear but was enhanced at higher indium compositions. Figure 3(b) shows $I_{PL}^{0^\circ}$, $I_{PL}^{90^\circ}$ and $I_{PL}^{90^\circ}/I_{PL}^{0^\circ}$ as a function of the thickness of the strain-reducing layer. As the thickness increased, $I_{PL}^{90^\circ}/I_{PL}^{0^\circ}$ increased. Above 6-8 nm, $I_{PL}^{90^\circ}/I_{PL}^{0^\circ}$ seemed to become saturated. It should be noted that the saturation point was almost the same as the QD height.

Figures 3(a) and 3(b) clearly indicate that the strain-reducing layer improved the anisotropic polarization features. We considered that the results relate to the shape of the wavefunction in the QDs. The strain-reducing layer lowers the height of the confinement potential barrier, and the indium composition and the thickness directly determine the barrier height. Considering that the polarization depends on the carrier confinement direction, we supposed that the change of the barrier height influenced the

symmetry of the carrier confinement.

3. Calculation of Wavefunction

To explore the origin of the improvement of symmetry in the polarization, we theoretically evaluated the shape of the electron wavefunction in an InGaAs-buried InAs/GaAs QD. We studied the influence of the aspect ratio of the crystallographic QD structure and the parameters of the strain-reducing layer on the aspect ratio of the wavelength. Since the self-assembled QDs grown at the same time on the common substrate are expected to have similar characteristics, we think that the estimation for one QD can apply to the QD ensemble in the experiment.

The wavefunction of the self-assembled QD structures was computed using the three-dimensional finite element method based on the analytical continuum approach with which arbitrarily shaped QDs have been analyzed.[8, 17, 18] In the calculation, the domed and pyramidal QD structure was modeled to be grown on a GaAs substrate, embedded in a strain-reducing layer (see Figs. 4(a) and 4(b)), and capped by a GaAs layer. The indium composition was assumed to be 1 in both the QD and the wetting layer. To implement the computation, we divided the structure into cubes composed of six trigonal pyramidal voxels. The length of each side of the cubes was set to 1 nm. In the calculation, because the indium composition was averaged in the voxels and the voxel boundaries were not, in general, aligned with the QD

boundaries, the boundaries of the QD structure had a maximum uncertainty of 1 nm. First, we computed the strain distribution in the structure so that the strain energy had the minimum value. After estimating the strain distribution, we calculated the strain-induced modification of the band gap and the effective mass, and then solved the Schrödinger equation with the modification to obtain the wavefunction in the QD ground state. The procedure and used material parameters were based on those in ref. 8. In this study, we defined the major and minor axes of the QD structure and those of the wavefunction as L_{major}, L_{minor}, L^{Φ}_{major}, and L^{Φ}_{minor}, as shown in Figs. 4(a) - 4(c). Throughout the calculation, we assumed that L_{major} had a value of 20 nm and that the QD height was 10 nm.

Figures 5(a) and 5(b) indicate how much the symmetry was improved by the strain-reducing layer. The vertical axis indicates the aspect ratio of the minor axis to the major axis of the wavefunction. Several aspect ratios of the QD structure, i.e., L_{minor} / L_{major}, were assumed in the calculation, considering that the actual aspect ratios have been reported to be 0.89, 0.83, and 0.75.[11-13] The points at x = 0.5 with L_{minor} / L_{major} = 0.6 could not be calculated correctly in our system due to too much spread of the wavefunction. The characteristics are compared with those of the pyramidal QD and the domed QD.

Some characteristic features are shown in Figs. 5(a) and 5(b). The symmetry of the wavefunction is superior to that of the QD structure, even without the

strain-reducing layer (i.e., x = 0). The lower the QD symmetry, the greater the improvement in the symmetry. The wavefunction symmetry is better in the domed dot than in the pyramidal dot. In Fig. 5(a), we notice that the higher the indium composition of the strain-reducing layer, the better the resulting symmetry of the wavefunction. The improvement is not linear and is enhanced at higher indium compositions. The features are very similar to those in Fig. 3(a). In Fig. 5(b), we see that the improvement of the symmetry is enhanced by increasing the thickness of the strain-reducing layer. However, the enhancement is suppressed when the thickness exceeds the QD height. This finding explains well the results of the experiments shown in Fig. 3(b), where the improvement of symmetry becomes saturated when the thickness exceeds the QD height.

4. Discussion

We think that the permeation of the wavefunction into the vicinity of the QD explains the effect of the strain-reducing layer on the symmetry. Since L_{major} is smaller than the exciton Bohr radius, the wavefunction is not completely confined in the QD. The permeation is asymmetric in an asymmetric QD, i.e., the permeation in the minor axis direction is larger than that in the major axis direction.

The dependence of the symmetry improvement on the original structure's symmetry is summarized in Fig. 6(a). The difference in the aspect ratio between the

wavefunction and the QD structure is plotted as a function of L_{minor} / L_{major}. Figure 6(a) suggests that the permeation of the wavefunction is related to the symmetry improvement. It is clearly shown that the difference in the aspect ratio decreases in proportion to the increase in L_{minor}/L_{major}. Since L_{major} is common in these calculations, the increase of L_{minor} / L_{major} means the quantum confinement in the direction of the minor axis is reduced. We also see that the higher the indium composition of the strain-reducing layer, the greater the extent of symmetry improvement. The higher the indium composition, the lower the potential barrier height of the quantum confinement. Therefore, we can see that the wavefunction symmetry is better with a lower potential barrier.

To evaluate the asymmetric permeation of an electron wavefunction, we define the overflow rate as the probability amplitude outside the QD divided by the total probability amplitude as follows:

$$R_i^{\phi} = \frac{\left|\phi_i^{\text{outsideQD}}\right|^2}{\left|\phi_i^{\text{total}}\right|^2}, \qquad (1)$$

where the index i denotes the major axis and the minor axis, $\left|\phi_i^{\text{total}}\right|^2$ denotes the total probability amplitude at the cross section on the i axis, and $\left|\phi_i^{\text{outsideQD}}\right|^2$ denotes the part of $\left|\phi_i^{\text{total}}\right|^2$ outside the QD. Figure 6(b) shows the overflow rate, R_i^{ϕ}, as a function of

L_{minor} / L_{major}. R^{ϕ}_{major} is always smaller than R^{ϕ}_{minor}, and the difference between R^{ϕ}_{major} and R^{ϕ}_{minor} is larger as the indium compositions of surrounding layers increases. The behavior of the overflow rate agrees well with that of the improvement of symmetry presented in Fig. 6(a). This result suggests that the asymmetric permeation counterbalances the asymmetric QD structure and improves the symmetry of the wavefunction compared with that of the QD structure.

To predict the polarization of the light emission from QDs more precisely, we should consider some other aspects in addition to the shape of the wavefunction. One is the many-body concept. The photoluminescence from the excitons is affected by the interaction between the electrons and holes. Another is the properties of spin, where the polarizations arise. Actually, the zinc-blend lattice has no inversion symmetry, so crystalline directions force the alignment of the wavefunction. The piezoelectric charges due to strain may also further misalign the electrons and holes. We entrust the evaluation of these effects to future work.

In terms of practical applications, the strain-reducing layer must be designed bearing in mind that it affects the quantum efficiency and shifts the emission wavelength. As shown in Figs. 2(a) and 2(b), the emission intensity degraded with the peak shift when the net strain in the QD structure increased. The strain-reducing layers with $x \geq 0.19$ or $d \geq 12$ nm prevented room-temperature photon emission. It is well-known that high net strain in the QD structure enhances non-radiative

recombination.[15] In order to eliminate the grown-in defects and improve QD quantum efficiency, thermal treatment has been used during overgrowth and at postgrowth.[19] The quantum efficiency recovers at low temperatures. It should be noted that all the present semiconductor photon generators are cooled to liquid helium temperature to eliminate thermal noise. If we do not need to worry about the emission wavelength and the requirement of refrigerating the samples, embedding in a highly strained InGaAs layer is a very effective way to realize a symmetric wavefunction in an InAs QD state.

5. Conclusions

We report the linear polarization features of the vertical photoluminescence from InAs/GaAs self-assembled QDs embedded in an InGaAs strain-reducing layer. We found that the photoluminescence intensity depends on the polarization direction that is expected to originate in the structural asymmetry of the QD. The polarization dependence of the photoluminescence intensity was suppressed by the strain-reducing layer. The suppression was enhanced as the indium composition and thickness of the strain-reducing layer increased. Our calculations based on the three-dimensional finite element method suggest that the in-plane symmetry of the electron wavefunction is superior to that of the QD structure and that the strain-reducing layer further improves the wavefunction symmetry. The improvement in symmetry was explained by the in-plane anisotropic permeation of the wavefunction into the strain-reducing layer. Our

results will aid in the development of vertical-light-emitting QD devices such as surface-emitting lasers and entangled-photon generators.

Acknowledgements

The authors are grateful to Dr. Mitsuru Sugawara at Fujitsu Laboratories Ltd. for providing the QD samples and to Mr. Keita Watanabe for the fruitful discussion.

References

1) T. Kita, O. Wada, H. Ebe, Y. Nakata, and M. Sugawara : Jpn, J. Appl. Phys. **41** (2002) L1143.

2) K. Kawaguchi, N. Yasuoka, M. Ekawa, H. Ebe, T. Akiyama, M. Sugawara, and Y. Arakawa : Jpn. J. Appl. Phys. **45** (2006) L1244.

3) P. Jayavel, H. Tanaka, T. Kita, O. Wada, H. Ebe, M. Sugawara, J. Tatebayashi, Y. Arakawa, Y. Nakata, and T. Akiyama : Appl. Phys. Lett. **84** (2004) 1820.

4) K. Mukai and K. Nakashima : J. Nanosci. Nanotechnol. **6** (2006) 3705.

5) K. Nishi, H. Saito, S. Sugou, and J. S. Lee : Appl. Phys. Lett. **74** (1999) 1111.

6) C. Santori, M. Pelton, G. Solomon, Y. Dale, and Y. Yamamoto : Phys. Rev. Lett. **86** (2001) 1502.

7) T. Miyazawa, K. Takemoto, Y. Sakuma, S. Hirose, T. Usuki, N. Yokoyama, M. Takatsu, and Y. Arakawa : Jpn. J. Appl. Phys. **44** (2005) L620.

8) S. Noda, T. Abe, and M. Tamura : Phys. Rev. B **58** (1998) 7181.

9) Y. Nabetani, T. Ishikawa, S. Noda, and A. Sasaki : J. Appl. Phys. **76** (1994) 347.

10) Y.-W. Mo, D. E. Savage, B. S. Swartzentruber, and M. G. Lagally : Phys. Rev. Lett. **65** (1990) 1020.

11) H. Hwang, S. Yoon, H. Kwon, E. Yoon, H.-S. Kim, J. Y. Lee, and B. Cho : Appl. Phys. Lett. **85** (2004) 6383.

12) O. Benson, C. Santori, M. Pelton, and Y. Yamamoto : Phys. Rev. Lett. **84** (2000)

2513.

13) T. M. Stace, G. J. Milburn, and C. H. W. Barnes : Phys. Rev. B **67** (2003) 085317.

14) C. Santori, D. Fattal, M. Pelton, G. S. Solomon, and Y. Yamamoto : Phys. Rev. B **66** (2002) 045308.

15) K. Mukai, Y. Nakata, K. Otsubo, M. Sugawara, N. Yokoyama and H. Ishikawa : IEEE Photon. Technol. Lett. **11** (1999) 1205.

16) K. Otsubo, N. Hatori, M. Ishida, S. Okumura, T. Akiyama, Y. Nakata, H. Ebe, M. Sugawara, and Y. Arakawa : Jpn. J. Appl. Phys. **43** (2004) L1124.

17) H. J. Chu and J. Wang : J. Appl. Phys. **98** (2005) 034315, and references therein.

18) K. Mukai and Y. Nakatomi : J. Cryst. Growth **294** (2006) 268.

19) J. Tatebayashi, Y. Arakawa, N. Hatori, H. Ebe, M. Sugawara, H. Sudou, and A. Kuramata : Appl. Phys. Lett. **85** (2004) 1024.

Figure Captions

Figure 1　Cross-sectional TEM images of a self-assembled QD embedded in a 12-nm $In_{0.17}Ga_{0.83}As$ strain layer: (a) bright-field image and (b) dark-field image.

Figure 2　Photoluminescence spectra for two polarization directions as a function of (a) the indium composition and (b) the thickness of the strain-reducing layer.

Figure 3 Ratio of the photoluminescence intensities of the two polarization directions as a function of (a) the indium composition and (b) the thickness of the strain-reducing layer.

Figure 4 Definitions of L_{major} and L_{minor} of (a) a pyramidal and (b) a domed QD. (c) L^{Φ}_{major} and L^{Φ}_{minor} are defined by the projection of the wavefunction at half-maximum on the x-y plane.

Figure 5 Aspect ratio of the electron wavefunction as a function of (a) the indium composition and (b) the thickness of the strain-reducing layer.

Figure 6 (a) Difference in aspect ratio between the wavefunction and the QD structure as a function of the aspect ratio of the QD structure. (b) The overflow rate (defined in the text) as a function of the aspect ratio of the QD structure.

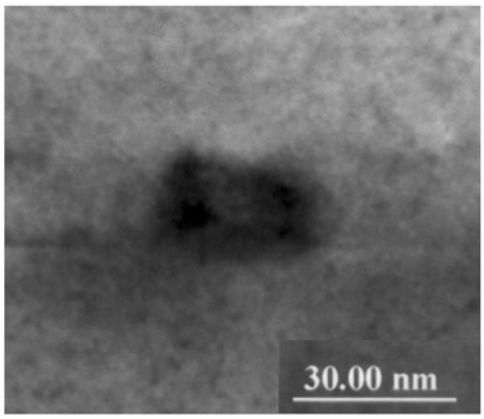

(a)

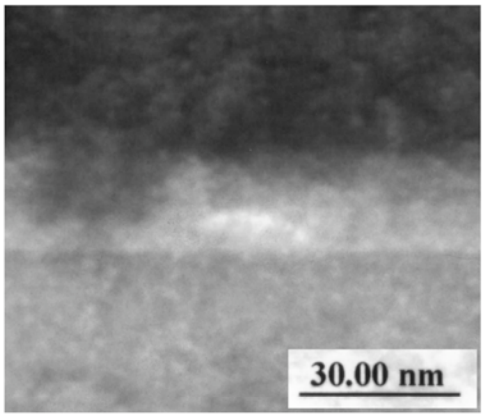

(b)

Figure 1

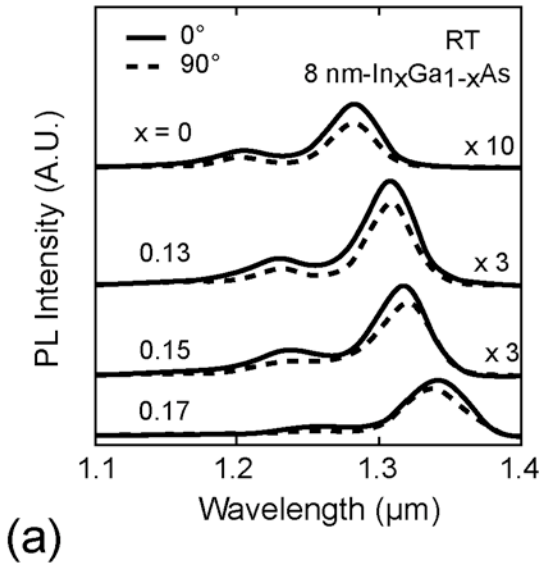
0°
90°
RT
8 nm-InxGa1-xAs
x = 0
x 10
0.13
x 3
0.15
x 3
0.17
PL Intensity (A.U.)
1.1
1.2
1.3
1.4
Wavelength (μm)

(a)

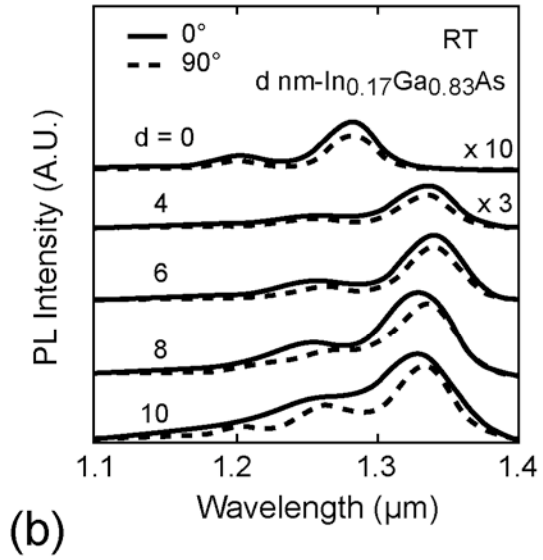
0°
90°
RT
d nm-In0.17Ga0.83As
d = 0
x 10
4
x 3
6
8
10
PL Intensity (A.U.)
1.1
1.2
1.3
1.4
Wavelength (μm)

(b)

Figure 2

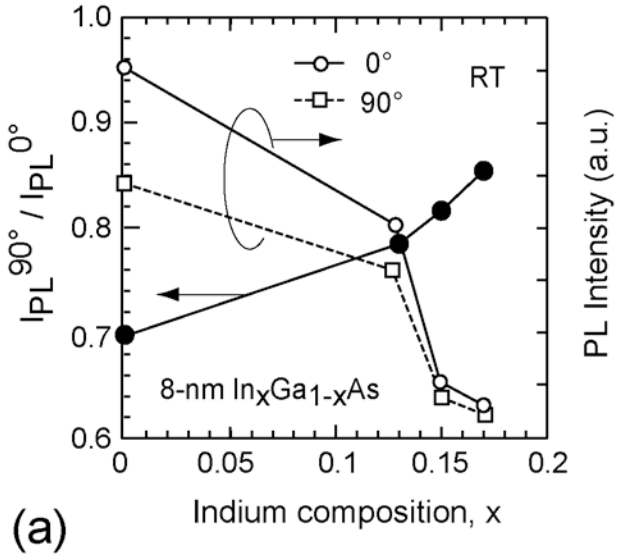
1.0
0.9
0.8
0.7
0.6
0
0.05
0.1
0.15
0.2
0°
90°
RT
8-nm InxGa1-xAs
IPL90° / IPL0°
PL Intensity (a.u.)
Indium composition, x

(a)

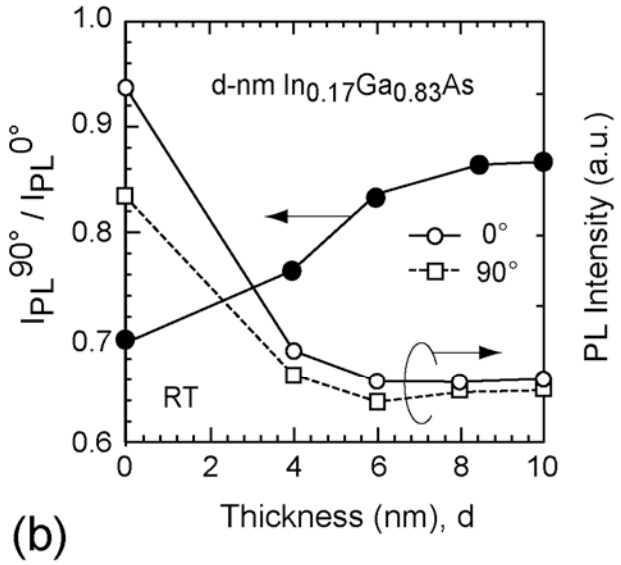
1.0
0.9
0.8
0.7
0.6
0
2
4
6
8
10
d-nm In0.17Ga0.83As
0°
90°
RT
IPL90° / IPL0°
PL Intensity (a.u.)
Thickness (nm), d

(b)

Figure 3

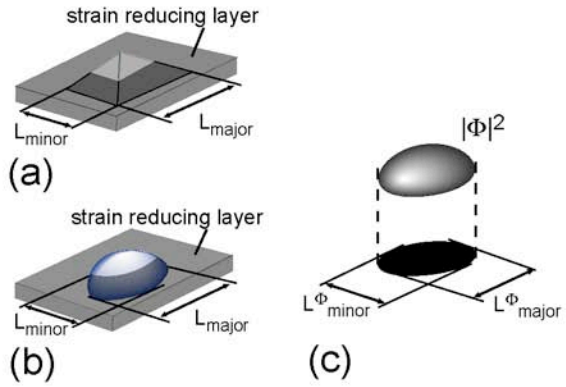
strain reducing layer
L_{minor}
L_{major}
(a)
strain reducing layer
L_{minor}
L_{major}
(b)
$|\Phi|^2$
L^{Φ}_{minor}
L^{Φ}_{major}
(c)

Figure 4

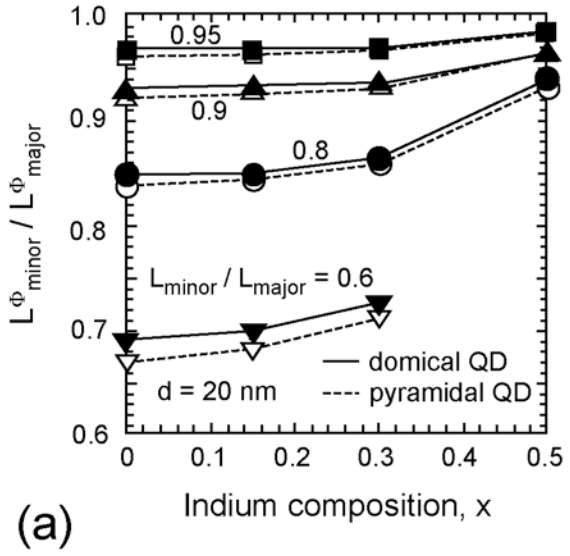
1.0
0.9
0.8
0.7
0.6
0.95
0.9
0.8
$L_{minor} / L_{major} = 0.6$
d = 20 nm
domical QD
pyramidal QD
$L^{\Phi}_{minor} / L^{\Phi}_{major}$
0
0.1
0.2
0.3
0.4
0.5
Indium composition, x

(a)

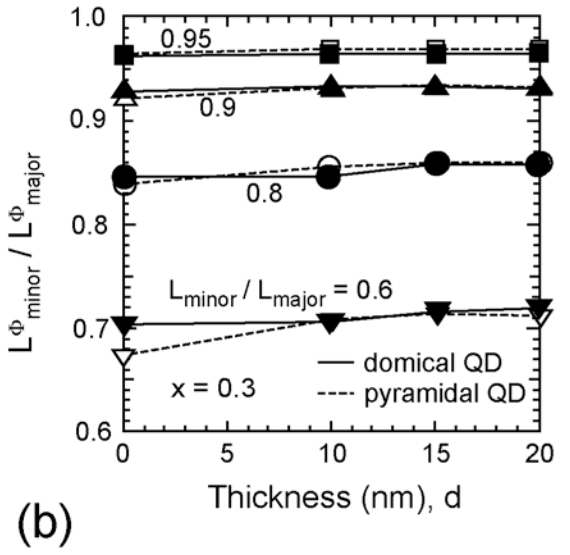
1.0
0.9
0.8
0.7
0.6
0.95
0.9
0.8
$L_{minor} / L_{major} = 0.6$
x = 0.3
domical QD
pyramidal QD
$L^{\Phi}_{minor} / L^{\Phi}_{major}$
0
5
10
15
20
Thickness (nm), d

(b)

Figure 5

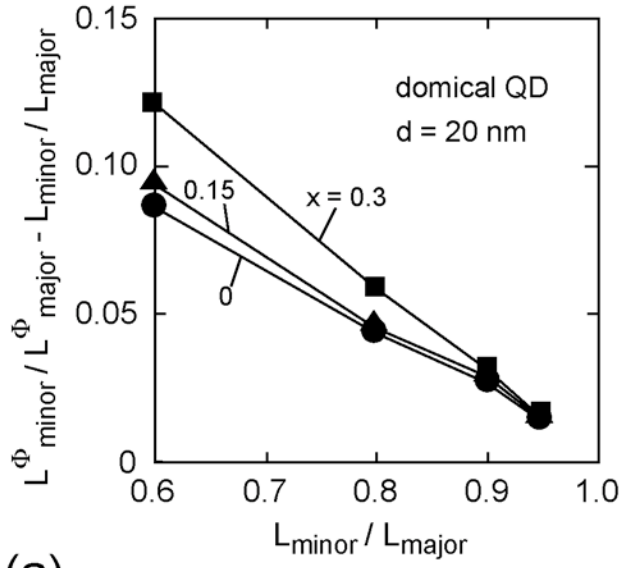
0.15
0.10
0.05
0
0.6
0.7
0.8
0.9
1.0
domical QD
d = 20 nm
x = 0.3
0.15
0
$L^{\Phi}_{minor} / L^{\Phi}_{major} - L_{minor} / L_{major}$
L_{minor} / L_{major}

(a)

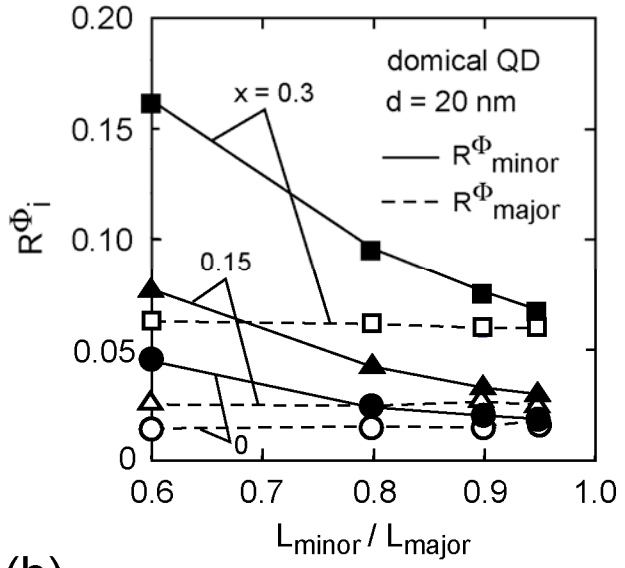
0.20
0.15
0.10
0.05
0
0.6
0.7
0.8
0.9
1.0
domical QD
d = 20 nm
x = 0.3
0.15
0
R^{Φ}_{minor}
R^{Φ}_{major}
R^{Φ}_{i}
L_{minor} / L_{major}

(b)

Figure 6